ACS OMEGA

Open Access

http://pubs.acs.org/journal/acsodf

Article

Antiurease Activity of Antibiotics: In Vitro, In Silico, Structure Activity Relationship, and MD Simulations of Cephalosporins and Fluoroquinolones

Misbah Aslam, Jameel Rahman,* Ambar Iqbal, Sara Mujtaba, Avinash Karkada Ashok, Farah Chafika Kaouche, Muhammad Munawar Hayat, Mouqadus-Un Nisa, and Muhammad Ashraf*

Cite This: *ACS Omega* 2024, 9, 14005−14016

Read Online

ACCESS | Metrics & More | Article Recommendations | Supporting Information

ABSTRACT: *Helicobacter pylori* infection is widespread in 50% of the world's population and is associated with gastric ulcers and related disorders that ultimately culminate in gastric cancer. Levofloxacin-based, or clarithromycin-based, triple therapy is frequently used to inhibit the bacterial urease enzyme for the eradication of *H. pylori*. A comprehensive investigation based on the urease inhibitory profiles of antibiotics and their computational implications is lacking in the scientific literature. The present study was aimed specifically to determine the antiurease activities within the realms of cephalosporins and fluoroquinolones by in vitro methods supported with in silico investigations. The results demonstrate the jack bean urease inhibitory activity of cephalosporins, wherein cefadroxil, cefpodoxime, cefotaxime, and cefaclor displayed inhibitions (IC_{50} 21.35 ± 0.64 to 62.86 ± 0.78 μM) compared with the standard thiourea (IC_{50} 21.25 ± 0.15 μM). Among fluoroquinolones, levofloxacin, ofloxacin, and gemifloxacin (IC_{50} 7.24 ± 0.29 to 16.53 ± 0.85 μM) unveiled remarkable inhibitory profiles. Levofloxacin and ofloxacin exhibited competitive inhibition against the said enzyme. Ciprofloxacin and moxifloxacin displayed weak urease inhibitions. During molecular docking studies, Asp362, Gly279, Arg338, Asn168, Asp223, Gln364, and Met366 were involved in hydrogen bonding in fluoroquinolones, and hydrogen bonding was established with Arg338, His248, Asn168 residues, and metal Ni601 and Ni602 of the enzyme. MD simulations and MMPBSA results demonstrated the existence of significant protein−ligand binding. Overall, these results warrant further investigations into the significance of these active molecules in relation to their inhibitory potential against the targeted urease enzyme.

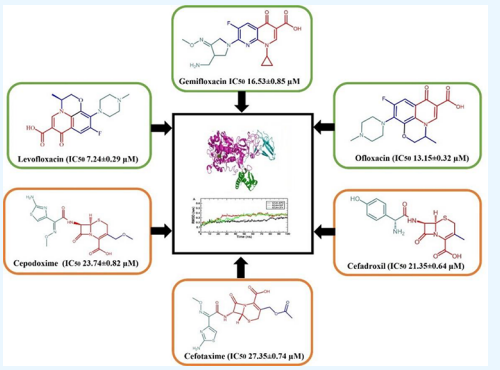

1. INTRODUCTION

Helicobacter pylori (HP) infection is prevalent in about 1/2 of the world's population and is an etiological agent linked with peptic ulcer, gastric cancer, gastric mucosa-associated lymphoid tissue lymphoma, and gastric adenocarcinoma.[1] HP is a microaerophilic Gram-negative bacteria associated with non-gastric diseases, including iron-deficiency anemia and idiopathic thrombocytopenic purpura.[2] Various treatment regimens include triple therapy, quadruple therapy, sequential therapy, and levofloxacin-based triple therapy that should eradicate HP up to 90% (Table 1). HP infection is treated by combination therapy of antibiotics and bismuth salt that has a role in combating the infection and promoting ulcer healing. Bismuth salts create a protective barrier on the ulcer site, reducing inflammation and allowing the antibiotics to target and eliminate the HP more efficiently. By combining the bactericidal action of antibiotics, e.g., metronidazole, clarithromycin, amoxicillin, levofloxacin, and tetracycline, with the therapeutic properties of bismuth salts, this treatment regimen provides a comprehensive approach to eradicate HP infection and facilitates the recovery of peptic ulcers (Figure 1). Nonetheless, the class of antibiotics and their duration of treatment promote serious side effects, including gastrointestinal disturbances and other complications even involving liver and kidney toxicity.[3] A recent systematic and meta-analysis of clinical trial review has demonstrated that the quadruple therapy was found to be more effective (82% eradication rate) than triple therapy (74% eradication rate) as the first line treatment, but little differences were noticed when quadruple therapy was used in the second-line treatment, taking into consideration the other relevant risk factors (Table 1).[4] Recently, different types of probiotics have been reported for reducing the side effects of adjuvant anti-HP therapy and increasing the HP eradication rates in various combinations

Received: November 23, 2023
Revised: February 22, 2024
Accepted: March 1, 2024
Published: March 14, 2024

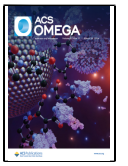

Table 1. Summary of Treatment Regimens against HP Urease; the Dose of the Drug, Duration, Toxicity, or Allergy Response are Monitored by the Physician[4]

therapy	drug components
first line regimens	clarithromycin triple:[a] PPI, clarithromycin, amoxicillin, metronidazole
	bismuth quadruple: PPI, bismuth subcitrate, bismuth subsalicylate, metronidazole, tetracycline
	nonbismuth-based quadruple: PPI, clarithromycin, amoxicillin, metronidazole
	vonoprazan, amoxicillin or amoxicillin, clarithromycin
alterative	sequential: PPI, clarithromycin, amoxicillin, metronidazole
salvage regimen	hybrid: PPI, clarithromycin, amoxicillin, metronidazole
levofloxacin containing alterative/salvage regimen	levofloxacin-based: PPI, levofloxacin, amoxicillin
	levofloxacin sequential: levofloxacin, amoxicillin, metronidazole
	LOAD: PPI, levofloxacin, alinia (nitazoxanide), doxycycline or metronidazole

[a]PPI = proton pump inhibitors (esomeprazole, lansoprazole, omeprazole, pantoprazole, rabeprazole, and dexlanoprazole).

and at different doses and durations. *Limosilactobacillus reuteri* has been found to be an effective probiotic for HP treatment. Clinical guidelines recommend different first-line treatment depending upon antimicrobial resistance patterns in each region, and the most relevant selection of antibiotics, suppression of acid secretion, and observance to therapy are factors affecting the effective eradication of HP.[5]

Over 1 million new cases of gastric cancer and 800,000 deaths occurred in 2020 due to HP-related gastric cancer.[6] It has been observed by WHO that HP strains are resistant to clarithromycin, metronidazole, and levofloxacin by >15% worldwide.[7] *H. pylori* survives in the acidic pH of stomach because of its production of urease enzyme, which hydrolyzes urea into ammonia, thus forming a protective ammonia blanket around itself (Figure 1). In response to this basic environment, the stomach produces a large amount of acid that damages its own mucous layers, eventually causing gastric or peptic ulcers which ultimately may lead to cancer. Studies have indicated that such cancers rank fourth among the most prevalent cancers and are the second leading cause of cancer-related mortality worldwide.[8] WHO classifies HP as a class 1 carcinogen.[9] Studies have shown a vast majority of strains displaying variations in genome sequencing up to 20%.[10] Epidemiological studies explicated that several genetic components, like CagA gene product, were linked with the development of gastroduodenal diseases, chronic atropic gastritis, and peptic ulcers.[11] It has recently been reported that the anti-HP activity was linked to inhibiting the phosphorylation of CagA protein.[12] Further, there is strong evidence that urease also plays a significant role in the deactivation of complement of the host-defense mechanism.[13] Resultantly, urease inhibition is now seriously considered the primary treatment against HP infection.

Urease is a metalloenzyme that is found in plant and bacterial species, e.g., jack bean and *H. pylori*. Nickel ions in the active site of urease facilitate the conversion of urea to ammonia and carbon dioxide.[14] When urease activity is elevated during urea fertilization in soil, a significant quantity of urea is transformed into gaseous ammonia which results in an escalation of ammonia toxicity in the atmosphere, leading to both economic issues and nutrient deprivation for plants.[15] This released ammonia has also played a very significant role in health issues such as kidney as well as urinary tract stone,[16] pyelonephritis, and hepatic coma.[17]

Antibiotics either kill or impede the growth of bacteria, thus aiding in both the prevention and treatment of infectious diseases.[19] Various classes of antibiotics have been reported based on chemical structure, range of effectiveness, and

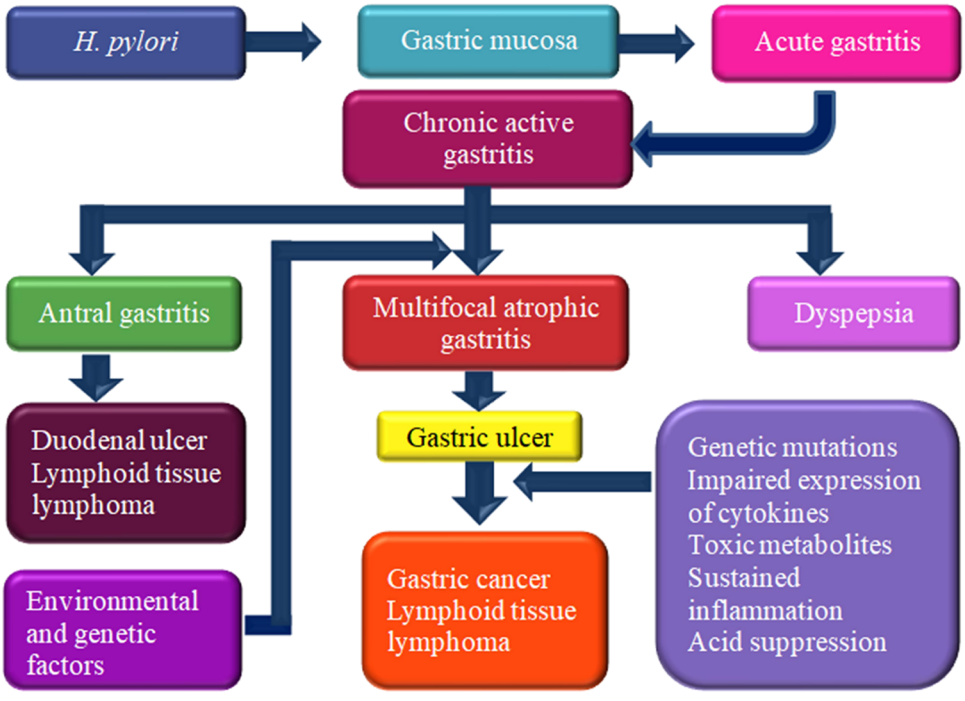

Figure 1. Summary of events from *H. pylori* infection to the development of the disease.

https://doi.org/10.1021/acsomega.3c09355
ACS Omega 2024, 9, 14005−14016

Table 2. Classification of Cephalosporin and Fluoroquinolone Antibiotics Based on Target Action Sites[18]

sr. no.	classification based on the mechanism of action	class	examples
1	cephalosporins inhibit cell wall synthesis via inhibition of synthesis of peptidoglycan	1st generation	cefalexin, cefradine, cefadroxil
		2nd generation	cefaclor, cefprozil, cefuroxime
		3rd generation	cefixime, cefotaxime, ceftriaxone, cefoperazone, ceftazidime, ceftizoxime, cefpodoxime
		4th generation	cefepime
2	fluoroquinolones inhibit DNA synthesis via DNA gyrase	1st generation	nalidixic acid
		2nd generation	levofloxacin, rufloxacin, nadifloxacin, ofloxacin, ciprofloxacin, norfloxacin
		3rd generation	sparfloxacin, gatifloxacin
		4th generation	moxifloxacin, gemifloxacin

Table 3. JB Urease Inhibition Studies of Cephalosporins and Fluoroquinolones; Data are Mean ± SEM, n = 3−4[a]

sr. no.	antibiotic	inhibition (%) at 0.25 mM	IC_{50} (μM)	no. of assays (n)	r^2	95% CI (min−max)	p-value
1	cefalexin	72.53 ± 0.94	145.85 ± 0.37	3	0.976		
2	cefradine	54.86 ± 1.54	226.83 ± 0.95	3	0.978		
3	cefadroxil	91.27 ± 0.85	21.35 ± 0.64	4	0.985	19.84−23.68	0.035
4	cefaclor	92.43 ± 1.53	62.86 ± 0.78	4	0.979	57.71−67.35	0.137
5	cefuroxime	51.68 ± 1.56	241.54 ± 0.87	3	0.985		
6	cefprozil	42.76 ± 0.27		3			
7	cefixime	68.54 ± 1.85	215.47 ± 0.76	3	0.985		
8	ceftriaxone	72.57 ± 0.98	157.35 ± 0.42	3	0.985		
9	cefoperazone	34.54 ± 0.26		3			
10	ceftazidime	76.94 ± 1.57	123.58 ± 0.19	3	0.985		
11	cefpodoxime	91.35 ± 1.86	23.74 ± 0.82	4	0.998	21.84−25.46	0.018
12	ceftizoxime	32.41 ± 0.24		3			
13	cefotaxime	81.93 ± 1.46	27.35 ± 0.74	4	0.991	25.26−29.03	0.006
14	cefepime	73.26 ± 1.35	78.65 ± 0.45	4	0.989	76.58−79.10	0.102
15	ceftazidime	49.52 ± 1.78		3			
16	levofloxacin	81.92 ± 0.62	7.24 ± 0.29	4	0.978	6.55−8.64	<0.0001
17	ofloxacin	83.67 ± 0.67	13.15 ± 0.32	4	0.988	11.64−14.79	<0.0001
18	ciprofloxacin	78.35 ± 0.85	134.52 ± 0.52	3	0.969		
19	sparfloxacin	57.59 ± 0.62	213.86 ± 0.32	3	0.989		
20	gemifloxacin	92.48 ± 1.35	16.53 ± 0.85	4	0.990	15.11−17.31	<0.0001
21	moxifloxacin	75.27 ± 0.74	134.27 ± 0.39	3	0.979		
thiourea (standard)		98.21 ± 0.18	21.25 ± 0.15	4	0.995	20.32−22.17	

[a]Statistical parameters were calculated only for the active molecules by the GraphPad Prism software v. 5.0 with built-in statistical analysis module. p-values were determined as compared with the standard thiourea.

mechanism of action (Table 2), such as β-lactam antibiotics, e.g., penicillin, sulphonamides, rifamycins, streptogramins, tetracyclines, and fluoroquinolones.[20] These agents exhibit bactericidal effects by selectively targeting cell wall/cell membrane or inhibiting specific enzymes or processes within the bacteria and have capability to resist biofilm formation.[21] This class includes penicillin derivatives, cephalosporins, monobactams, and carbapenems.[22] These antibiotics work by irreversibly inhibiting the activity of transpeptidase, an enzyme that is utilized by bacteria to construct their cell walls. The final step in peptidoglycan synthesis involves the action of transpeptidase, specifically penicillin binding proteins (PBPs), which bind to the D-Ala-D-Ala region of muropeptides (peptidoglycan precursors) to facilitate cross-linking of the peptidoglycan structure. Fluoroquinolones exert their action by disrupting the replication and transcription processes of bacterial DNA. They achieve this by stabilizing the interaction between DNA and gyrases/topoisomerases, which are essential enzymes involved in DNA replication (Table 1). Quinolones function by transforming their intended targets, specifically gyrase and topoisomerase IV, into harmful enzymes that cause fragmentation of the bacterial chromosome.[23]

1.1. Rationale of the Study. The antibiotics in various combinations of therapeutic regimens along with proton pump inhibitors and other medications are used in the eradication of *H. pylori* for the treatment of peptic ulcers and related disorders. In-depth literature surveys revealed no published data on the in vitro and in silico investigations of the urease inhibitory profiles of the commonly used antibiotics. It was therefore hypothesized that these antibiotics may have more potential to eradicate *H. pylori* by inhibiting urease as the target enzyme. For this purpose, we screened over 50 standard antibiotics by in vitro methods against the JB urease and by in silico methods against the HP urease enzyme since it is

https://doi.org/10.1021/acsomega.3c09355
ACS Omega 2024, 9, 14005−14016

established that JB urease inhibitors are also excellent HP urease inhibitors. The present paper therefore describes the results of only two classes of antibiotics, cephalosporins and fluoroquinolones. The work on the other antibiotics is in progress and will be published separately.

2. RESULTS AND DISCUSSION

2.1. Urease Inhibition and SAR Studies of Cephalosporins. Cephalosporins exhibited good inhibitory activity (Table 3 and Figures 2 and 3). Cefadroxil, cefpodoxime, and

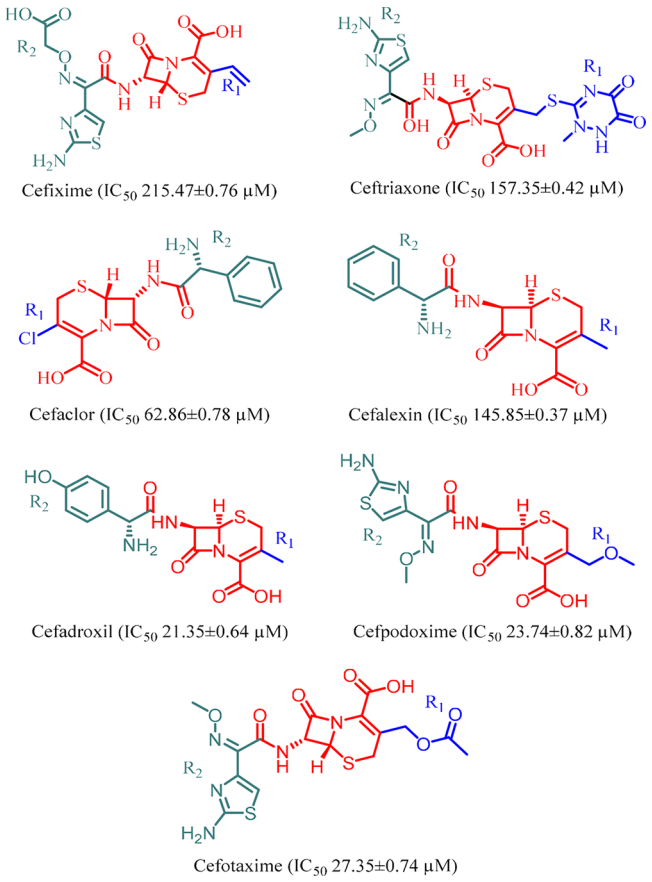

Figure 2. Inhibitory profiles and SAR analyses of cephalosporins. The core structure is shown in red. Blue and greenish structures represent various R groups attached to main skeleton.

cefotaxime were the most active among these antibiotics with IC_{50} values of 21.35 ± 0.54 μM ($p < 0.035$), 23.74 ± 0.82 μM ($p < 0.018$), and 27.35 ± 0.74 μM ($p < 0.006$), respectively, as compared to thiourea (21.25 ± 0.15 μM). Cefaclor and cefepime both exhibited moderately good urease inhibitory profiles with IC_{50} values of 62.86 ± 0.78 and 78.65 ± 0.45 μM, respectively. Cefalexin, ceftriaxone, and cefixime showed poor inhibitory potential (Table 3 and Figures 2 and 3). Cefadroxil was active against urease enzyme due to the presence of a methyl group attached to the central ring at position R_1 and 4-(aminomethyl)phenol group at position R_2. Cefpodoxime has a methoxyethane group at position R_1 and (*Z*)-1-(2-aminothiazol-4-yl)ethan-1-one O-methyl oxime group at position R_2, while cefotaxime possessed ethyl acetate at position R_1 and (*Z*)-1-(2-aminothiazol-4-yl)-1-(methoxyimino)propan-2-one at position R_2. Cefaclor showed good activity against the said enzyme due to the presence of a −Cl group attached at the core ring as R_1 and a phenylethane amine group as R_2. Cefpodoxime urease inhibition was also comparable to cefaclor due to the methoxyethane group present at position R_1, while the (*Z*)-2-aminothiazole-4-carbaldehyde O-methyl oxime part was present at position R_2 (Figures 2 and 3). When R_1 was replaced with methyl group keeping the R_2 same, IC_{50} value increased to 145.85 ± 0.37 μM as in cefalexin. The excellent activity of cefaclor is demonstrated by the electron withdrawing effect of the chloro group compared with that of the electron donating methyl group in cefalexin. Cefixime has vinyl group as R_1 and amino-thiazole and acetic acid groups attached to amide carbon of the core skeleton as R_2 and its poor inhibitory activity (IC_{50} 215.47 ± 0.76 μM) may be due to steric hindrance of bulky R_2 group compared with that of phenylethane amine group found in cefaclor and cefalexin. In ceftriaxone, the incorporation of methylthio group linked with triazine ring as R_1 and oxime group attached with amino-thiazole ring as R_2 resulted in improved activity (IC_{50} 157.35 ± 0.42 μM) like that of cefalexin (IC_{50} 145.85 ± 0.37 μM) than that of cefixime (IC_{50} 215.47 ± 0.76 μM). These results display that the type and class of R_1 group attached to core ring determines the inhibitory potential of cephalosporins as urease inhibitors (Table 3 and Figures 2 and 3).

2.2. Urease Inhibition and SAR Studies of Fluoroquinolones. Fluoroquinolones contain a basic carboxylated quinoline core ring attached with different substituents (Table 3 and Figure 4). SAR analysis of these antibiotics unveiled that levofloxacin and ofloxacin were the most active urease inhibitors with IC_{50} values of 7.24 ± 0.29 and 13.15 ± 0.32 μM, respectively, as compared with the standard thiourea ($p < 0.0001$) (Table 3). Both of these antibiotics are isomers and contain −F group attached to dimethylchromane ring at position R_1 and piperazine ring at position R_2 (Figure 4). By assessing their activity, it is ascertained that the *S*-configuration in levofloxacin showed higher urease inhibition as compared to the *R*-configuration containing ofloxacin molecule. The inhibition studies of levofloxacin (IC_{50} 7.24 ± 0.29 μM) and ciprofloxacin (IC_{50} 134.52 ± 0.52 μM) demonstrated that both structures were similar except six-membered oxazino core in levofloxacin that contributed to enhanced activity more than highly ring-strained isopropyl group at quinoline moiety of ciprofloxacin. Gemifloxacin also showed excellent enzyme inhibition activity (IC_{50} 16.53 ± 0.85 μM) due to the presence of fluoropyridine ring at position R_1 and (E)-4-(aminomethyl)-1l2-pyrrolidin-3-one O-methyl oxime at position R_2 (Figure 4). It exhibited highly significant inhibition as compared to thiourea ($p < 0.0001$).

By comparing the activity of sparfloxacin (IC_{50} 213.86 ± 0.32 μM) and ciprofloxacin, it was revealed that piperazine ring in ciprofloxacin was unsubstituted while sparfloxacin had substituted piperazine ring which contributed to steric effects resulting in decreased inhibitory profiles against the enzyme (Figure 4). The substituted piperazine and quinoline rings in sparfloxacin with two −F groups reduced the binding capabilities in the establishment of interactions in the active pocket of the enzyme, while ciprofloxacin easily managed hydrogen bonding with the target enzyme. Ciprofloxacin (IC_{50} 134.52 ± 0.52 μM) and moxifloxacin (IC_{50} 135.27 ± 0.39 μM) had little difference in their IC_{50} values, wherein the main difference arises at R_2, piperazine ring present in ciprofloxacin, while pyrrolo and pyrimidine ring in moxifloxacin was important. Other antibiotics displayed poor enzyme inhibitory profiles.

https://doi.org/10.1021/acsomega.3c09355
ACS Omega 2024, 9, 14005−14016

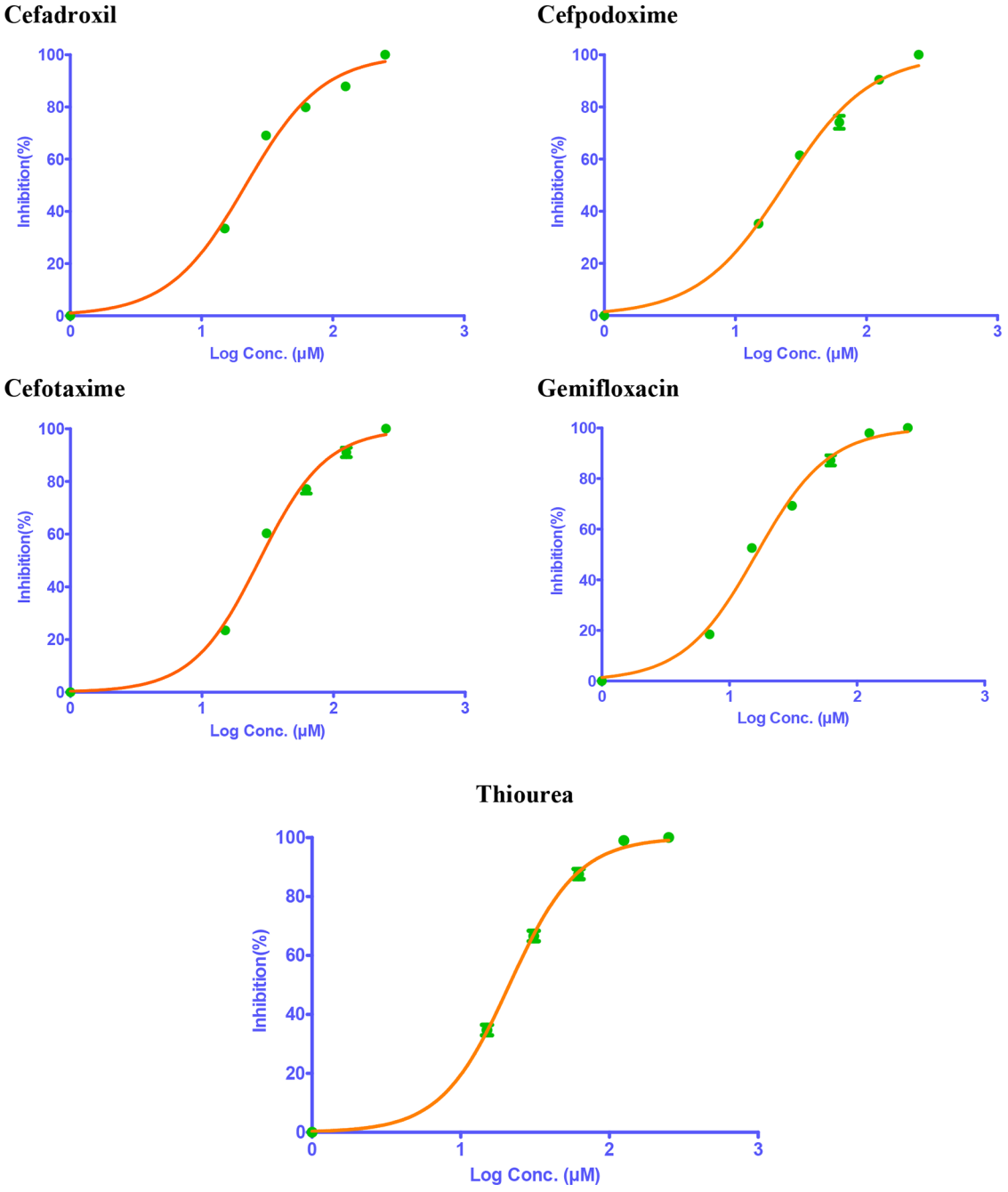

Figure 3. JB urease inhibition (%) profiles vs log of concentrations of cefadroxil, cefpodoxime, cefotaxime, gemifloxacin, and standard thiourea.

2.2.1. Kinetic Analysis of Fluoroquinolones. Kinetic assays of two potent urease inhibitors ofloxacin and levofloxacin were carried out to evaluate their affinity and velocity of reaction, and both antibiotics were found to be competitive inhibitors of the JB urease enzyme (Figure 5). Slight differences were observed in the kinetic parameters of these two isomers (Table 4 and Figure 5). Levofloxacin achieved maximum velocity of 84.51 μm/min with less substrate concentration as compared to ofloxacin as depicted by K_m of 7.390 μM. Levofloxacin also had lower inhibitory constant value of 4.914 μM that was agreed with its IC_{50} value of 7.24 $\pm$ 0.29 μM.

2.3. Molecular Docking Studies. The active site of the protein in its bound state is represented in Figure 6. The comprehensive binding interactions of the most active cephalosporin (cefadroxil) and fluoroquinolone (levofloxacin) in the active pocket of JB urease are shown in Figures 7 and 8, whereas the binding energies of the active inhibitors are shown in Tables 5 and 6. The binding free energies and ligand–receptor interaction profiles demonstrated good correlation with the experimental results.

2.3.1. Cefadroxil-HP Urease. In the molecular docking analysis, cefadroxil successfully docked in the active site of HP urease with a binding free energy of −7.6 kcal/mol (Table 5 and Figure 7). Within this active site, the amino group of Arg338 plays a pivotal role by donating its hydrogen, resulting in the formation of three hydrogen bonds: two of these bonds are established with the oxygen atoms of the carboxylic group, while the third bond is formed with the carbonyl moiety of the carboxylic group adjacent to the beta-lactam ring. Additionally, the amino group of His248 actively participates in hydrogen

https://doi.org/10.1021/acsomega.3c09355
ACS Omega 2024, 9, 14005−14016

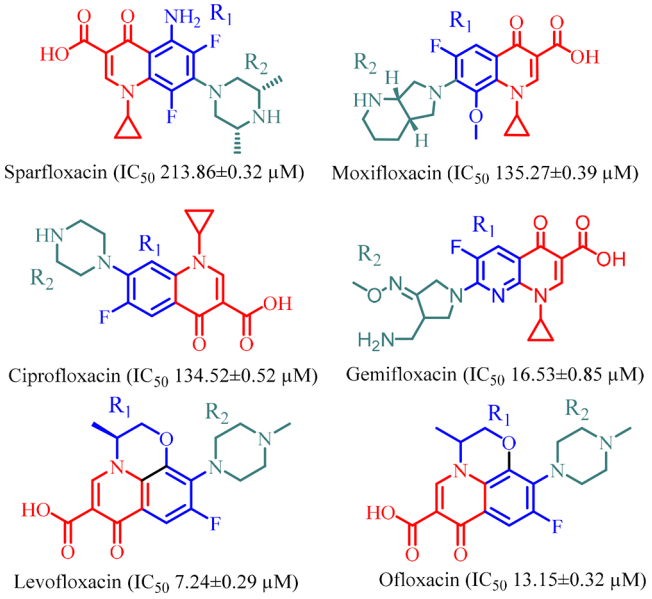

Figure 4. Inhibitory profiles and SAR analysis of the fluoroquinolones. The core structure is shown in red and blue and greenish structures represent various R groups attached to main skeleton.

bonding, by donating its hydrogen to the carboxylic group of cefadroxil. Furthermore, the nitrogen atom within the amino acetamide group donates its hydrogen to the oxygen of Asn168, further contributing to the intricate network of hydrogen bonding interactions. Notably, His136, His138, Ala169, Kcx219, His221, Glu222, Asp223, Thr251, Gly279, Gly280, Leu318, Cys321, His322, Phe334, Ala365, and Met366 exhibit hydrophobic interactions with the cefadroxil molecule (Table 5 and Figure 7).

2.3.2. Levofloxacin-HP Urease. Levofloxacin (*S* isomer of ofloxacin) was docked in the active pocket of HP urease with a binding free energy of −7.4 kcal/mol (Table 6 and Figure 8). In the molecular docking analysis against HP urease with the levofloxacin drug, several crucial interactions were observed. The Asp362 amino acid residue established a hydrogen bond with the carbonyl moiety of the carboxylic group adjacent to the dihydropyridine ring of levofloxacin, with a bond length of 2.86 Å, signifying a key interaction for stabilizing the drug within the enzyme's active site. Additionally, a network of residues, including Asn168, Ala169, Kcx219, Glu222, His221, Asp223, His274, Gly280, Cys321, His322, Arg338, Ala365, Met366, Ni601, and Ni602, engaged in hydrophobic interactions with levofloxacin (Figure 8). These interactions played a crucial role in enhancing the drug's binding and potentially influencing its inhibitory effect on the HP urease enzyme.

2.4. Molecular Dynamics Simulation. To explore the stability of the protein in its bound state with the ligands, the systems were simulated for a chemical time of 100 ns. The protein in its unbound state with the ligands was also simulated to establish a comparative MD analysis to investigate the role of the ligand in stabilizing the protein. The generated MD trajectory was subjected to calculation of the root-mean-square deviation (RMSD) of the backbone atoms of the protein. Figure 9A,B represents the RMSD plot for biomolecular systems.

The violin plot indicates that the average RMSD for 6ZJA-APO complex to be 0.23, 0.35 nm for 6ZJA-CEF and 6ZJA-LEV complexes with the highest density around the averages. The RMSD plots in Figure 9A,B indicate that the trajectories have stabilized beyond 50 ns and the trends are reasonably stable. These stable trajectories were considered for further analyses.

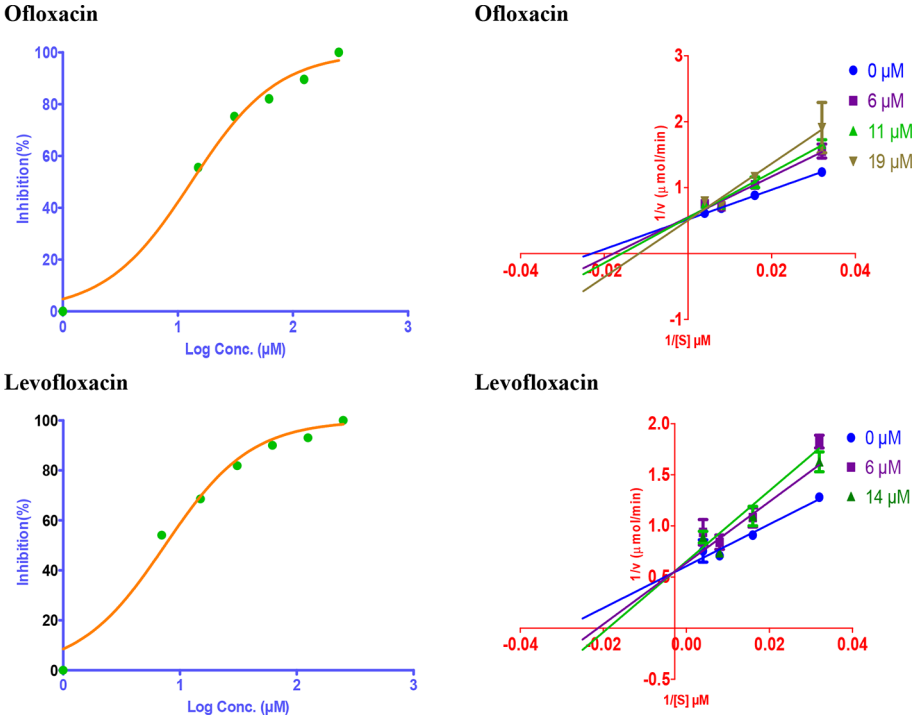

Figure 5. JB urease inhibition (%) profiles vs logarithm of antibiotic concentration and double reciprocal plots to determine the mode of inhibition and other kinetic parameters of ofloxacin and levofloxacin. Details are given in the text. Data is mean ± SEM, $n = 3$.

https://doi.org/10.1021/acsomega.3c09355
ACS Omega 2024, 9, 14005−14016

Table 4. Kinetic Properties of Ofloxacin and Levofloxacin against the BJ Urease Enzyme during In Vitro Assays

sr. no.	antibiotic	inhibition (%) at 0.25 mM	IC_{50} (μM)	K_i (μM)	K_m (μM)	V_{max} (μM/min)	type of inhibition
1	ofloxacin	83.67 ± 0.67	13.15 ± 0.32	5.433	13.531	86.62	competitive
2	levofloxacin	81.92 ± 0.62	7.24 ± 0.29	4.914	7.390	84.51	competitive
thiourea (standard)		98.21 ± 0.18	21.25 ± 0.15	19.65	23.92	110.1	competitive

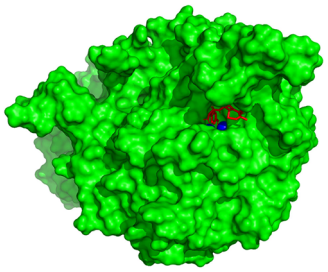

Figure 6. Representation of cefadroxil and levofloxacin in the active pocket of the enzyme (ID: 6ZJA). The protein surface is represented in green while the ligand (red) and nickel ion (blue) are hosted at the active site of the enzyme.

The residue by residue fluctuations were studied by fitting them to the MD trajectory and observing the root-mean-square fluctuation (RMSF). Residues 310−354, a helix−loop−helix is an active site flap as explained by ref 24. The RMSF plot in Figure 10 indicates that the active site flap fluctuates at a relatively higher degree in the 6ZJA-APO complex (0.467 nm) than the protein−ligand systems (0.35 nm). This might hint at the stabilizing effect of the ligand on the active site residues.

The active site nickel ion of the native form of 6ZJA projected significant random motions at the active site in comparison to those of the protein ligand systems (Figure 11A). This suggests conformational instability at the active site in 6ZJA-APO complex. To visualize the hydrogen bonds between the ligands and the protein, the hydrogen bond evolution was calculated (Figure 11B). The MD input structure for 6ZJA-CEF complex had hydrogen bonds between cefadroxil and His274, Arg338, His248 and Asn168 of urease, which seems to be maintained throughout the simulation. Though not significant, with making and breaking, there also seems to exist hydrogen bonds between receptor (ID 6ZJA) and the ligand levofloxacin.

Solvent accessible surface area (SASA) quantifies the portion of the protein that interfaces with the surrounding solvents within a simulation box. In our current investigation, the protein SASA depicted (Figure 12A) displays variations that center around a relatively stable mean value. For the apoprotein form of the receptor (ID: 6JZA) and the 6JZA-CEF complex, SASA averages were approximately 243.43 and 244.22 nm^2, respectively. In contrast, the 6JZA-LEV complex exhibited a slightly higher mean SASA value, approximately 250.26 nm^2, indicating a more extended protein conformation.

Further, we conducted a radius of gyration (R_g) analysis to assess the structural characteristics of the protein in the three studied systems, as illustrated in Figure 12B. The R_g analysis allows us to quantify the distribution of mass relative to the center of mass of the protein, which provides valuable insights into the structural compactness or expansion of the protein. In the initial 16 ns of the simulation, both the 6JZA-CEF and 6JZA-LEV systems exhibited R_g values that were lower than the R_g values of the 6JZA-APO, indicating the compact structure adapted by the protein in complex with levofloxacin and cefadroxil. However, as the simulation progressed, we observed a noticeable increase in the R_g values of both the 6JZA-LEV and 6JZA-CEF complexes. This increase indicates that the protein adopts a more expanded structural conformation when in complex with levofloxacin and cefadroxil, in contrast to its more compact form in the apoprotein configuration.

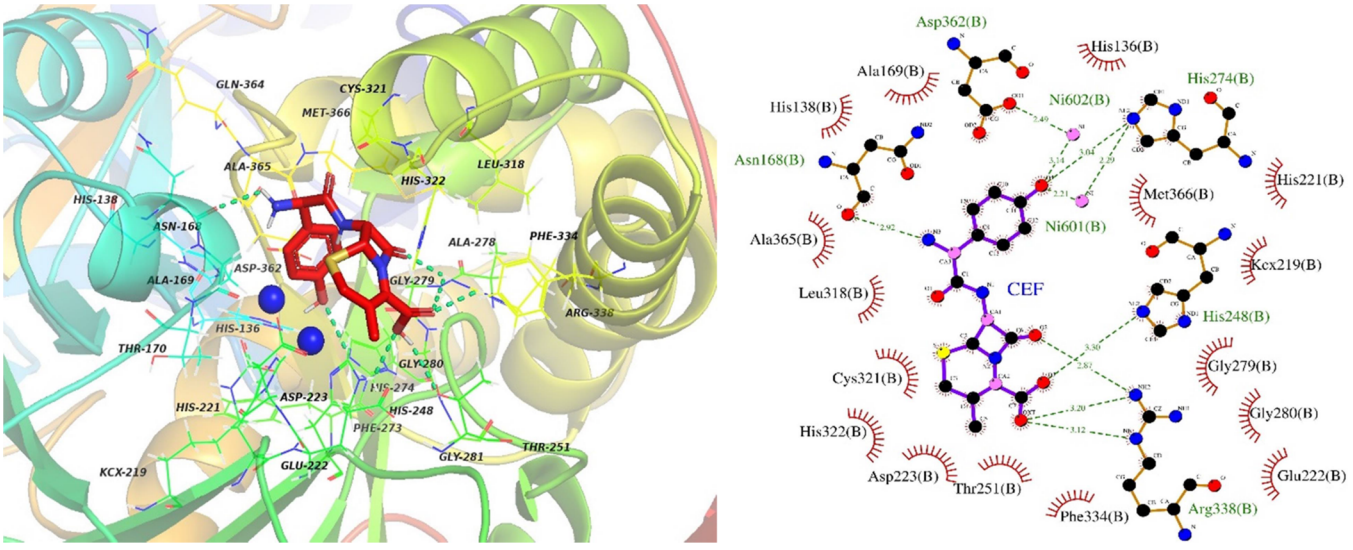

Figure 7. 2D and 3D binding interactions of CEF (cefadroxil) with HP urease (PDB ID: 6ZJA). The interaction map for the protein−ligand complexes was generated through LigPlot+ (PubMed ID: 21919503). The hydrogen bonds are represented as dotted bonds, while the hydrophobic interactions are represented as red rays.

https://doi.org/10.1021/acsomega.3c09355
ACS Omega 2024, 9, 14005−14016

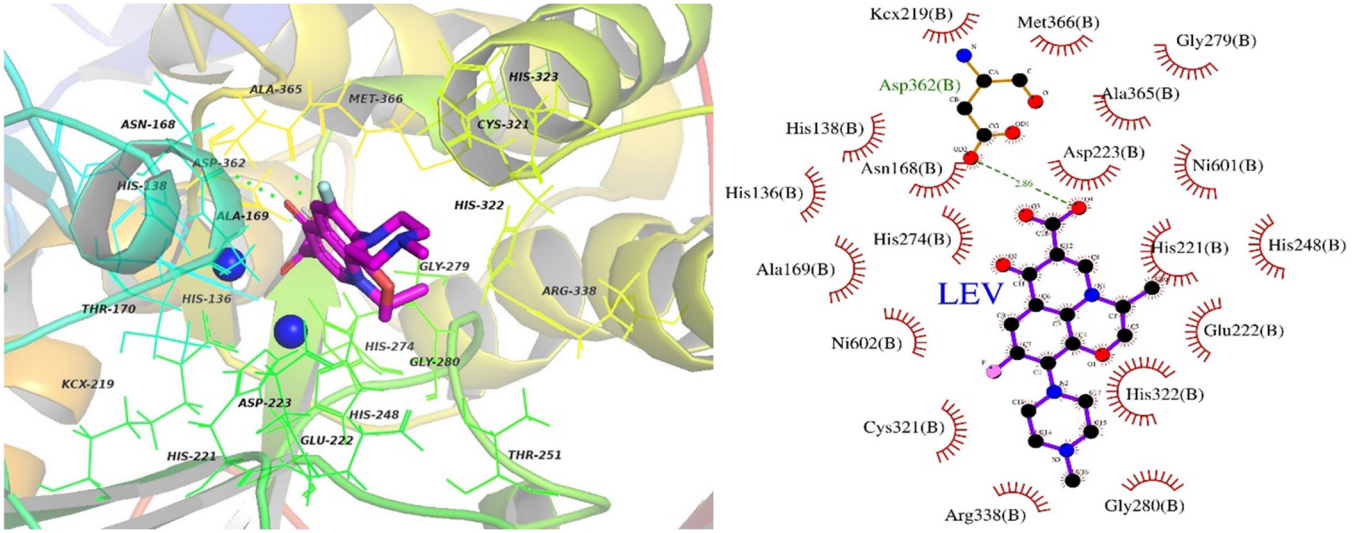

Figure 8. 2D and 3D binding interactions of LEV (levofloxacin) with HP urease (PDB ID: 6ZJA). The interaction map for the protein−ligand complexes was generated through LigPlot+. The hydrogen bonds are represented as dotted bonds, while the hydrophobic interactions are represented as red rays.

Table 5. Molecular Interaction Analysis of Cephalosporins Active against the HP Urease

sr. no.	antibiotics	binding free energy (kcal/mol)	hydrogen bond interactions	hydrophobic interactions
1	cefadroxil	−7.6	His248 (3.30 Å), Asp362 (2.49 Å), His274 (274 Å), Arg338 (3.12 Å, 3.20 Å, 2.87 Å), Ni601 (2.21 Å), Ni602 (3.14 Å)	Ala169, Kcx,219, His221, Glu222, Asp223, Thr251, Gly279, Gly280, Leu318, Cys321, His322, Phe334, Ala365, Met366
2	cefaclor	−7.0	Asp223 (3.23 Å)	Ala169, His221, Glu222, His248, Thr251, Ala278, Gly279, Gly280, Met317, Leu318, Cys321, His322, Phe334, Arg338, Ala365, Met366
3	cefpodoxime	−6.9	Asn169 (3.0 Å), Ala278 (3.34 Å), Arg338 (3.06 Å)	Asp165, Ala169, Glu222, Asp223, His248, Thr251, Gly279, Gly280, His314, Met317, Leu318, Cys321, His322, Ile339, Ala365, Met366
4	cefotaxime	−6.5	Ala169 (3.17 Å), His221 (3.09 Å), Thr251 (3.14 Å), Arg338 (3.13 Å)	Asn168, Glu222, His248, Gly279, Gly280, Met317, Val320, Cys321, His322, Phe334, Gln364, Ala365, Met366

Table 6. Molecular Interaction Analysis of Fluoroquinolones Active against the HP Urease

sr. no.	antibiotics	binding free energy (kcal/mol)	hydrogen bond interactions	hydrophobic interactions
1	levofloxacin	−7.4	Asp362 (2.86 Å)	Asn168, Ala169, Kcx219, Glu222, His221, Asp223, His274, Gly280, Cys321, His322, Arg338, Ala365, Met366, Ni601, Ni602
2	ofloxacin	−7.1	Gly279 (2.88 Å) Arg338 (2.80 Å)	Asn168, Ala169, Glu222, His248, Ala278, Gly280, Met317, Leu318, Cys321, His322, Gln364, Ala365, Met366
3	gemifloxacin	−7.0	Asn168 (3.06 Å), Asp223 (3.15 Å), Gln364 (2.80 Å), Met366 (3.09 Å)	His138, Ile140, Ala169, Kcx219, His221, Glu222, His248, Thr251, His274, Gly279, Gly280, Met317, Cys321, His322, Arg338, Asp362, Ala365

2.5. Binding Free Energy Calculations. We conducted an in-depth examination of the binding affinities between the ligands and the urease enzyme, focusing on elucidating the accessibility of the binding site. To better understand the nature of the interaction between the ligands and the protein, as well as to investigate the relative affinity of the ligands to the protein-binding site and gain insights into the contribution of the ligands to specific residues, we employed binding-free energy calculations (Table 7). For the designated binding-free energy calculations, we employed the MD-based molecular mechanics/Poisson−Boltzmann surface area (MM/PBSA) approach, utilizing the MMPBSA[25] tool in the GROMACS software suite. Representative frames were meticulously selected and recorded for each energy term calculation, and the free energy calculation was performed over the course of 100 ns of time. Notably, it is imperative to highlight that 6ZJA-CEF exhibited a substantial binding affinity for the protein (−23.051 ± 41.746 kJ/mol), as did 6ZJA-LEV (−13.591 ± 26.072 kJ/mol) (Table 7). This observation suggests that the binding site likely facilitates complexation of the ligands.

3. CONCLUSIONS

The present studies revealed the maximal inhibitory potential of fluoroquinolone levofloxacin (IC_{50} 7.24 ± 0.29 μM) and ofloxacin (IC_{50} 13.15 ± 0.32 μM), which presented competitive inhibition of the JB urease with K_i values of 4.914 and 5.433 μM, respectively, while other fluoroquinolones, including ciprofloxacin and moxifloxacin, were weak enzyme inhibitors. This study elucidates the crucial roles played by Asp362, Gly279, Arg338, Asn168, Asp223, Gln364, and Met366 in establishing hydrogen bonds with fluoroqui-

https://doi.org/10.1021/acsomega.3c09355
ACS Omega 2024, 9, 14005−14016

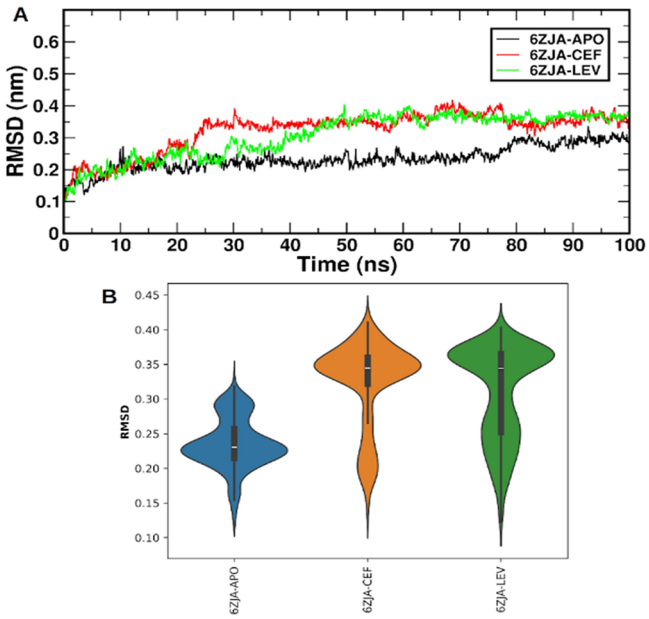

Figure 9. RMSD plot for the trajectories. (A) Frame by frame backbone comparison of the backbone residues with the reference structure. (B) Violin plot for the RMSD data in nm.

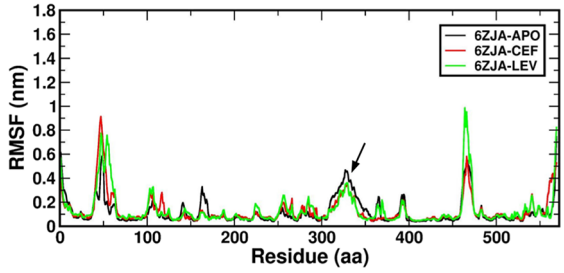

Figure 10. RMSF plot for the MD trajectory. The regions that form coils or loops experience higher degrees of fluctuations. The arrow represents the active site flap.

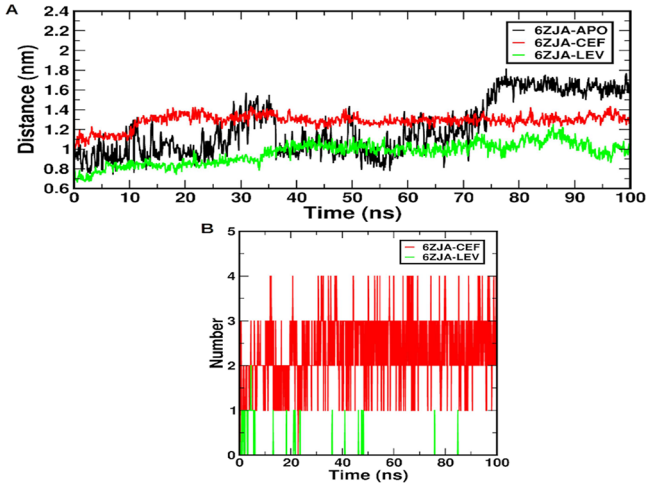

Figure 11. Distance between the nickel ion at the active site (A). The hydrogen bond graph between the urease enzyme and the ligands is indicated in (B).

nolones. Among cephalosporins, cefadroxil and cefaclor were the most active drugs. Cefadroxil formed hydrogen bonds with Arg338, His248, and Asn168 residues, as well as with metal ions Ni601 and Ni602 in the enzyme, and the binding free energy was calculated to be −7.6 kcal/mol, indicating strong interactions and stabilization of the drug within the enzyme's active site. MD simulation analysis discovered stable protein−ligand complexes with significant binding between the protein and the ligand, as estimated through MMPBSA. RMSD and RMSF values supported the binding profiles of receptor−ligand complexes with the maintenance of stable hydrogen bonding throughout the simulation. SASA analysis revealed slightly more extended receptor conformation for levofloxacin (250.26 nm^2) than cefadroxil (244.22 nm^2) or apoprotein (243.43 nm^2). Radius of gyration indicated more compact complexes at 16 ns simulation, and slightly expanded conformation was recorded as it progressed. Overall, the present study indicated that the active antibiotics should carefully be investigated during in vivo studies and careful demonstration by the clinicians is recommended since the in vitro and in silico soundings are in no way otherwise alternatives. Further investigations are necessitated for repurposing of drugs as antiurease agents, and work is in progress on these lines.

4. MATERIALS AND METHODS

4.1. Materials. All chemicals including enzymes, substrates, and standards of analytical grade were purchased from Sigma-Aldrich. Standard antibiotics were a kind gift from Punjab Drug Testing Laboratory, Lahore and Multan Drug Testing Laboratory, Multan (Pakistan), with >99% purity. For the preparation of solutions, HPLC-grade methanol was used.

4.2. Urease Inhibitory Assay. Urease inhibition assay was performed as reported.[26] The reaction mixture of 200 μL in a 96-well plate contained 50 mM phosphate buffer pH 7.4, 10 μL of test solution, and 10 μL of jack bean (JB) urease enzyme solution (1 unit/well). The contents were mixed and preincubated for 10 min at 37 °C. After the given time, 20 μL of 50 mM urea solution was added and incubation continued for a further 15 min. The reaction was stopped by the addition of 70 μL of freshly prepared phenol-alkali reagent. The contents were read at 630 nm after 10 min using a 96-well plate reader (Synergy HTX BioTek, USA). Assays were performed using both positive (thiourea) and negative controls. Data was expressed as mean ± SEM, n = 3−4. The urease activity was expressed using the following formula.

$$\text{Urease inhibition (\%)} = (\text{Abs. of control} - \text{Abs. of test solution}/\text{Abs. of control}) \times 100$$

Serial dilutions of the active solutions were prepared, and their inhibitory profiles were determined. Determination of IC_{50} values of active molecules, kinetic analysis, and nonlinear regression analysis was carried out using built-in module in GraphPad Prism v. 5.0 software.

4.3. Molecular Docking Studies. *4.3.1. Structure Preprocessing and Validation.* The 3D structure of the urease enzyme with the inhibitor bound at the active site (PDB ID: 6ZJA) was downloaded from the Protein Data Bank.[27] The structure was preprocessed by removing the water molecules and active site inhibitor. Further, hydrogen atoms were added, and the model was subjected to validation on the UCLA-DOE LAB SAVES v6.0 server (https://saves.mbi.ucla.edu/).

https://doi.org/10.1021/acsomega.3c09355
ACS Omega 2024, 9, 14005−14016

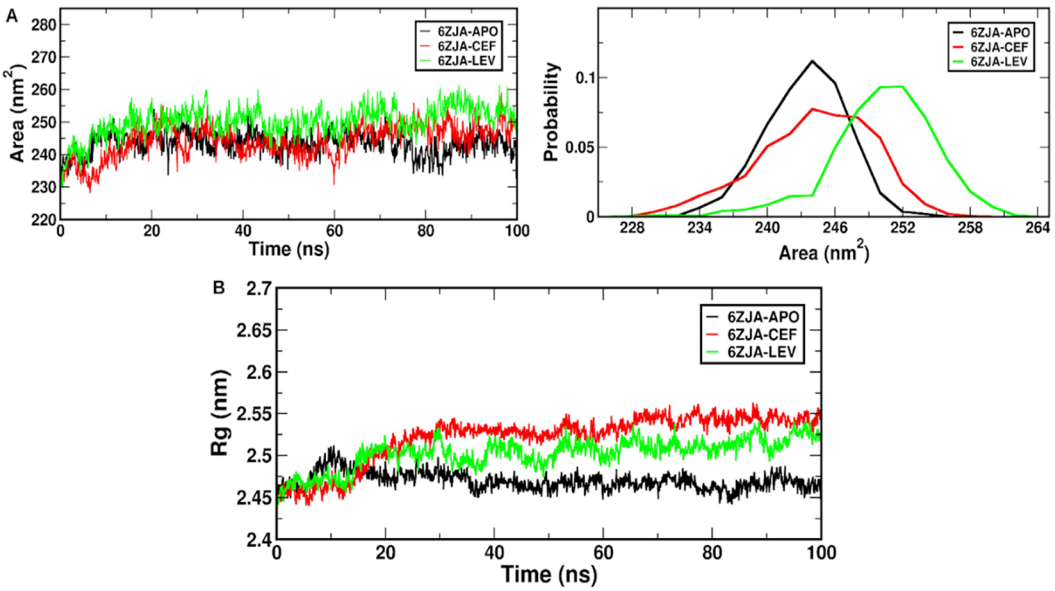

Figure 12. (A) SASA plot for the systems and its corresponding probability distribution. The R_g plot is represented in (B).

Table 7. Summary of the Energy Contribution Estimated through MMPBSA

energy (kJ/mol)	6ZJA-CEF	6ZJA-LEV
Van der Waal energy	−0.799 ± 0.312	−68.604 ± 50.128
electrostatic energy	5.808 ± 4.686	47.157 ± 32.246
polar solvation energy	−28.260 ± 41.736	16.429 ± 48.548
SASA energy	0.199 ± 1.185	−8.573 ± 6.246
binding energy	−23.051 ± 41.746	−13.591 ± 26.072

For the prediction of the active site where the selected ligands can bind and interact within the active pocket of targeted proteins, i.e., JB urease using PDB ID: 6ZJA, AutoDock Vina with the Vina scoring function was employed. The cryogenic electron microscopy (Cryo-EM) structure, ID: 6ZJA, contains 569 amino acid residues and two nickel atoms at the active site. Secondary structure analysis of 6ZJA reveals its composition: 29.7% helices, 37.1% beta sheets, β sheet-associated residues, and 33.2% bends and coils. Notably, the structure is devoid of Ramachandran outliers, as shown in (Supporting Information, Figure S1) with an ERRAT quality score of 93.2331.

4.3.2. Preparation and Molecular Docking. The ligand 3D structures of cefadroxil (PubChem ID: 47965) and levofloxacin (PubChem ID: 149096) were downloaded from the PubChem database in the sdf format. These structures were energy-minimized using the universal force field on Avogadro and were converted to the pdbqt format using OpenBabel.[28] The protein structure was incorporated into the MGLTools 1.5.7 toolbox, and the grid box was set on the active site to perform active site-based molecular docking. The grid box dimensions were centered at 223.5 × 250.5 × 194.3 according to the *xyz* Cartesian coordinate system with a box size of 19.0 × 19.8 × 16.3. Further, with an exhaustiveness of 100, the docking was performed with AutoDock vina[29] with the Vina scoring function.

4.3.3. Molecular Dynamics Simulation. The molecular dynamics (MD) simulation was initiated using the GROMACS-2020.6 software suite compiled with CUDA dependency on Nvidia RTX 3060Ti GPU machines.[30] For this study, the optimal-docking scored models of three systems, namely, 6ZJA-cefadroxil (referred to as 6ZJA-CEF), 6ZJA-levofloxacin (referred to as 6ZJA-LEV), and the native 6ZJA (apoprotein) with nickel ions (referred to as 6ZJA-APO), were selected as the initial coordinates. To set up the simulation, each system was solvated using a three-points (TIP3P) water model, and they were enclosed within cubic periodic boundary conditions.[31] The dimensions of this box were defined as 100 × 100 × 100, ensuring a minimum of 10 Å of space between the protein and each side of the 3D box, following the approach outlined.[32] The parameters for the ligands cefadroxil and levofloxacin were generated using the CGenFF tool by CHARMM.[33] Under physiological conditions with a pH of 7.0, MD simulations were conducted under specific conditions. Periodic boundary conditions were employed to account for the protein residues in their expected ionization states. To neutralize the entire complex, a Monte Carlo ion-placing method, as described by ref 34 was utilized. A force constant of 1000 kJ/mol nm^2 was consistently applied throughout all three stages of the MD simulation to restrict the movement of heavy atoms and maintain the native protein folding, following the methodology as outlined.[34] The first step involved optimizing the geometry of each system, which was achieved by performing 5000 iterations of the steepest descent technique over 5 ps (ps). Subsequently, a two-stage equilibration process was performed, with 100,000 (100 ps) conditioning iterations for each stage. The initial equilibration phase employed a constant NVT ensemble (controlling the number of particles, volume, and temperature), with temperature control applied using the Berendsen temperature-coupling method, in accordance with ref 35. The second equilibration stage utilized the Parrinello−Rahman Barostat within an NPT ensemble (constant number of particles, pressure, and temperature) set to 1 atm and 303.15 K, following the guidelines as mentioned.[36]

For computing interactions during the 100 ns (ns) of MD simulations, the Particle Mesh Ewald (PME) technique, as described by Darden et al. in 1993,[37] was employed. Given the need for stable nanosecond trajectories in highly polar macromolecules like proteins, all covalent bond lengths,

https://doi.org/10.1021/acsomega.3c09355
ACS Omega 2024, 9, 14005−14016

including hydrogen bonds, were constrained using the linear constraint LINCS technique, and the integration time step was set to 2 fs (fs), following Hess et al. method.[38] The Verlet cutoff approach was used to handle Coulomb (electrostatic potential), Lennard-Jones (Pauli repulsion and hydrophobic/van der Waals attractions), and nonbonded interactions within a 10 Å cutoff range, as per Pall and Hess's recommendation.[39] The CHARMM36m all-atom force field was applied to represent the ions and protein in the MD simulation. Postsimulation analysis was performed using GROMACS built-in capabilities, enabling the assessment of various parameters, including RMSD, RMSF, the radius of gyration (Rg), SASA, and hydrogen-bond interactions.

■ ASSOCIATED CONTENT

Supporting Information

The Supporting Information is available free of charge at https://pubs.acs.org/doi/10.1021/acsomega.3c09355.

Ramachandran plot of the enzyme (PDF)

■ AUTHOR INFORMATION

Corresponding Authors

Jameel Rahman − *Institute of Chemistry, B.J. Campus, The Islamia University of Bahawalpur, Bahawalpur 36000, Pakistan*; Email: jameel.rehman@iub.edu.pk

Muhammad Ashraf − *Institute of Chemistry, B.J. Campus, The Islamia University of Bahawalpur, Bahawalpur 36000, Pakistan*; orcid.org/0000-0002-7994-8720; Email: dr.m.ashraf@gmail.com

Authors

Misbah Aslam − *Institute of Chemistry, B.J. Campus, The Islamia University of Bahawalpur, Bahawalpur 36000, Pakistan*

Ambar Iqbal − *Institute of Chemistry, B.J. Campus and Department of Biochemistry and Molecular Biology, Institute of Biochemistry, Biotechnology, Bioinformatics (IBBB), B.J. Campus, The Islamia University of Bahawalpur, Bahawalpur 36000, Pakistan*

Sara Mujtaba − *Institute of Chemistry, B.J. Campus, The Islamia University of Bahawalpur, Bahawalpur 36000, Pakistan*

Avinash Karkada Ashok − *Department of Biotechnology, Siddaganga Institute of Technology, Tumakuru 572103 Karnataka, India*

Farah Chafika Kaouche − *Department of Chemistry, Faculty of Sciences of Mater, Ibn Khaldoun University, 14000 Tiaret, Algeria*

Muhammad Munawar Hayat − *P & SH Department, Punjab Drug Testing Laboratory, Lahore 631000, Pakistan*

Mouqadus-Un Nisa − *Multan Drug Testing Laboratory, near Multan Institute of Kidney Disease, Multan 261000, Pakistan*

Complete contact information is available at: https://pubs.acs.org/10.1021/acsomega.3c09355

Author Contributions

M.A., J.R., M.A., and M.M.H.: conceptualization. M.A. and S.M.: methodology and lab work. A.I., A.K.A., and F.C.K.: in silico studies. M.A., J.R., M.A., S.M., M.M.H., A.I., A.K.A., and M.N.: writing, review editing, and data analysis. J.R. and M.A.: supervision. M.M.H. and M.N.: resources.

Notes

The authors declare no competing financial interest.

■ ACKNOWLEDGMENTS

The authors are thankful to colleagues in Punjab Drug Testing Laboratory (DTL) Lahore and the Multan Drug Testing Laboratory, Multan, Pakistan for providing the standard antibiotics for the present studies.

■ REFERENCES

(1) Sivri, B. Trends in peptic ulcer pharmacotherapy. *Fundamental & clinical pharmacology* **2004**, *18* (1), 23−31. Srisuphanunt, M.; Wilairatana, P.; Kooltheat, N.; Duangchan, T.; Katzenmeier, G.; Rose, J. B. Molecular Mechanisms of Antibiotic Resistance and Novel Treatment Strategies for Helicobacter pylori Infections. *Tropical Medicine and Infectious Disease* **2023**, *8* (3), 163.

(2) Cunha, B. A. Antibiotic side effects. *Medical Clinics of North America* **2001**, *85* (1), 149−185. Howson, C. P.; Hiyama, T.; Wynder, E. L. The decline in gastric cancer: epidemiology of an unplanned triumph. *Epidemiologic reviews* **1986**, *8* (1), 1−27.

(3) Bayerdorffer, E.; Ottenjann, R. The role of antibiotics in Campylobacter pylori associated peptic ulcer disease. *Scand. J. Gastroenterol.* **1988**, *23* (sup142), 93−100. Couce, A.; Blazquez, J. Side effects of antibiotics on genetic variability. *FEMS Microbiology Reviews* **2009**, *33* (3), 531−538.

(4) Myran, L.; Zarbock, S. D. Management of Helicobacter pylori infection. *US Pharm.* **2018**, *43* (4), 27−32. Kiani, F.; Khademolhosseini, S.; Mohammadi, J.; Tavasol, A.; Hajibeygi, R.; Fathi, M.; Dousti, M. Novel Information Regarding the Treatment of Helicobacter pylori Infection: A Systematic Review and Meta-analysis of Randomized Clinical Trials. *Current Reviews in Clinical and Experimental Pharmacology Formerly Current Clinical Pharmacology* **2024**, *19* (2), 184−203. Liu, L.; Nahata, M. C. Vonoprazan with amoxicillin or amoxicillin and clarithromycin for the treatment of Helicobacter pylori infection. *Ann. Pharmacother.* **2023**, *57*, 1185−1197, DOI: 10.1177/10600280221149708.

(5) Liang, B.; Yuan, Y.; Peng, X.-J.; Liu, X.-L.; Hu, X.-K.; Xing, D.-M. Current and future perspectives for Helicobacter pylori treatment and management: From antibiotics to probiotics. *Frontiers in Cellular and Infection Microbiology* **2022**, *12*, 1740.

(6) Sung, H.; Ferlay, J.; Siegel, R. L.; Laversanne, M.; Soerjomataram, I.; Jemal, A.; Bray, F. Global cancer statistics 2020: GLOBOCAN estimates of incidence and mortality worldwide for 36 cancers in 185 countries. *CA: A Cancer Journal for Clinicians* **2021**, *71* (3), 209−249.

(7) Savoldi, A.; Carrara, E.; Graham, D. Y.; Conti, M.; Tacconelli, E. Prevalence of antibiotic resistance in Helicobacter pylori: a systematic review and meta-analysis in World Health Organization regions. *Gastroenterology* **2018**, *155* (5), 1372−1382.e1317.

(8) Parkin, D. M.; Bray, F.; Devesa, S. Cancer burden in the year 2000. The global picture. *Eur. J. Cancer* **2001**, *37* (37), 4−66.

(9) Smoot, D. T.; Elliott, T. B.; Verspaget, H. W.; Jones, D.; Allen, C. R.; Vernon, K. G.; Bremner, T.; Kidd, L. C. R.; Kim, K. S.; Groupman, J. D. Influence of Helicobacter pylori on reactive oxygen-induced gastric epithelial cell injury. *Carcinogenesis* **2000**, *21* (11), 2091−2095.

(10) Ernst, P. B.; Peura, D. A.; Crowe, S. E. The translation of Helicobacter pylori basic research to patient care. *Gastroenterology* **2006**, *130* (1), 188−206.

(11) Kusters, J. G.; Van Vliet, A. H.; Kuipers, E. J. Pathogenesis of Helicobacter pylori infection. *Clin. Microbiol. Rev.* **2006**, *19* (3), 449−490.

(12) Pandey, A.; Mishra, S.; Patra, A.; Somvanshi, P.; Bhavesh, N. S.; Chaturvedi, R. Role of curcumin's phenolic−OH group in the inhibition of Helicobacter pylori CagA phosphorylation. *J. Mol. Struct.* **2024**, *1296*, No. 136763.

(13) MacLaren, D. The significance of crease in Proteus pyelonephritis: a bacteriological study. *Journal of Pathology and*

https://doi.org/10.1021/acsomega.3c09355
ACS Omega 2024, 9, 14005−14016

Bacteriology **1968**, *96* (1), 45−56. Rautemaa, R.; Rautelin, H.; Puolakkainen, P.; Kokkola, A.; Karkkainen, P.; Meri, S. Survival of Helicobacter pylori from complement lysis by binding of GPI-anchored protectin (CD59). *Gastroenterology* **2001**, *120* (2), 470−479.

(14) Mazzei, L.; Cianci, M.; Benini, S.; Ciurli, S. The structure of the elusive crease-urea complex unveils a paradigmatic case of metallo-enzyme catalysis. *Angew. Chem. Int. Ed* **2019**, *58*, 7415−7419.

(15) Benini, S.; Rypniewski, W. R.; Wilson, K. S.; Miletti, S.; Ciurli, S.; Mangani, S. The complex of Bacillus pasteurii crease with acetohydroxamate anion from X-ray data at 1.55 Å resolution. *JBIC Journal of Biological Inorganic Chemistry* **2000**, *5*, 110−118. Seneviratne, G.; Van Holm, L.; Ekanayake, E. Agronomic benefits of rhizobial inoculant use over nitrogen fertilizer application in tropical soybean. *Field Crops Research* **2000**, *68* (3), 199−203.

(16) Wang, Z.; Zhang, Y.; Zhang, J.; Deng, Q.; Liang, H. Recent advances on the mechanisms of kidney stone formation. *Int. J. Mol. Med.* **2021**, *48* (2), 1−10.

(17) Arshad, T.; Khan, K. M.; Rasool, N.; Salar, U.; Hussain, S.; Asghar, H.; Ashraf, M.; Wadood, A.; Riaz, M.; Perveen, S. 5-Bromo-2-aryl benzimidazole derivatives as non-cytotoxic potential dual inhibitors of α-glucosidase and crease enzymes. *Bioorg. Chem.* **2017**, *72*, 21−31. Yang, W.; Feng, Q.; Peng, Z.; Wang, G. An overview on the synthetic crease inhibitors with structure-activity relationship and molecular docking. *Eur. J. Med. Chem.* **2022**, *234*, No. 114273.

(18) Etebu, E.; Arikekpar, I. Antibiotics: Classification and mechanisms of action with emphasis on molecular perspectives. *Int. J. Appl. Microbiol. Biotechnol. Res.* **2016**, *4*, 90−101, DOI: 10.33500/ijambr.2016.04.011. Kardos, N.; Demain, A. L. Penicillin: the medicine with the greatest impact on therapeutic outcomes. *Appl. Microbiol. Biotechnol.* **2011**, *92*, 677−687.

(19) Carta, F.; Scozzafava, A.; Supuran, C. T. Sulfonamides: a patent review (2008−2012). *Expert Opinion on Therapeutic Patents* **2012**, *22* (7), 747−758.

(20) Nasr, T.; Bondock, S.; Eid, S. Design, synthesis, antimicrobial evaluation and molecular docking studies of some new thiophene, pyrazole and pyridone derivatives bearing sulfisoxazole moiety. *Eur. J. Med. Chem.* **2014**, *84*, 491−504. Cimino, G.; Coates, R.; De Stefano, S.; Fontana, A.; Hemmerich, P.; Minale, L.; Rinehart, K.; Shield, L.; Sodano, G.; Toniolo, C. Chemistry of the Ansamycin Antibiotics. *Fortsch. Chem. Org. Naturst.* **1976**, *23*, 231−307. Mast, Y.; Wohlleben, W. Streptogramins−Two are better than one! *International Journal of Medical Microbiology* **2014**, *304* (1), 44−50. Chopra, I.; Roberts, M. Tetracycline antibiotics: mode of action, applications, molecular biology, and epidemiology of bacterial resistance. *Microbiology and Molecular Biology Reviews* **2001**, *65* (2), 232−260. Abdel-Aziz, S. A.; Cirnski, K.; Herrmann, J.; Abdel-Aal, M. A.; Youssif, B. G.; Salem, O. I. Novel fluoroquinolone hybrids as dual DNA gyrase and crease inhibitors with potential antibacterial activity: design, synthesis, and biological evaluation. *J. Mol. Struct.* **2023**, *1271*, No. 134049. Khan, F.; Pham, D. T.; Oloketuyi, S. F.; Kim, Y.-M. Antibiotics application strategies to control biofilm formation in pathogenic bacteria. *Current Pharmaceutical Biotechnology* **2020**, *21* (4), 270−286. Holten, K. B.; Onusko, E. M. Appropriate prescribing of oral beta-lactam antibiotics. *Am. Fam. Physician* **2000**, *62* (3), 611−620. Vollmer, W.; Blanot, D.; De Pedro, M. A. Peptidoglycan structure and architecture. *FEMS Microbiology Reviews* **2008**, *32* (2), 149−167.

(21) Bush, K. Characterization of beta-lactamases. *Antimicrob. Agents Chemother.* **1989**, *33* (3), 259−263.

(22) Jana, S.; Deb, J. Molecular understanding of aminoglycoside action and resistance. *Applied microbiology and biotechnology* **2006**, *70*, 140−150.

(23) Campoli-Richards, D. M.; Monk, J. P.; Price, A.; Benfield, P.; Todd, P. A.; Ward, A. Ciprofloxacin: a review of its antibacterial activity, pharmacokinetic properties and therapeutic use. *Drugs* **1988**, *35*, 373−447.

(24) Cunha, E. S.; Chen, X.; Sanz-Gaitero, M.; Mills, D. J.; Luecke, H. Cryo-EM structure of Helicobacter pylori crease with an inhibitor in the active site at 2.0 Å resolution. *Nature. Communications* **2021**, *12* (1), 230.

(25) Kumari, R.; Kumar, R.; Consortium, O. S. D. D.; Lynn, A. g_mmpbsa— A GROMACS tool for high-throughput MM-PBSA calculations. *J. Chem. Inf. Model.* **2014**, *54* (7), 1951−1962.

(26) Khan, M. U.; Aslam, M.; Shahzad, S. A.; Khan, Z. A.; Khan, N. A.; Ali, M.; Naz, S.; Rahman, J.; Farooq, U. Design and synthesis of thiobarbituric acid analogues as potent crease inhibitors. *J. Mol. Struct.* **2021**, *1231*, No. 129959.

(27) Hanwell, M. D.; Curtis, D. E.; Lonie, D. C.; Vandermeersch, T.; Zurek, E.; Hutchison, G. R. Avogadro: an advanced semantic chemical editor, visualization, and analysis platform. *Journal of Cheminformatics* **2012**, *4* (1), 1−17.

(28) Eberhardt, J.; Santos-Martins, D.; Tillack, A. F.; Forli, S. AutoDock Vina 1.2. 0: New docking methods, expanded force field, and python bindings. *J. Chem. Inf. Model.* **2021**, *61* (8), 3891−3898.

(29) Spoel, V. D. *GROMACS 2020.6 Source Code*. Zenodo. DOI: DOI: 10.5281/zenodo.4576055.

(30) Mark, P.; Nilsson, L. Structure and dynamics of the TIP3P, SPC, and SPC/E water models at 298 K. *J. Phys. Chem. A* **2001**, *105* (43), 9954−9960.

(31) Nayana, P.; Manjunatha, H.; Gollapalli, P.; Ashok, A. K.; Karal Andrade, P.; V, V. A combined in vitro and molecular dynamics simulation studies unveil the molecular basis of the anticancer potential of piperine targeting AKT1 against prostate cancer. *J. Biomol. Struct. Dyn.* **2023**, 1−14.

(32) Vanommeslaeghe, K.; Hatcher, E.; Acharya, C.; Kundu, S.; Zhong, S.; Shim, J.; Darian, E.; Guvench, O.; Lopes, P.; Vorobyov, I. CHARMM general force field: A force field for drug-like molecules compatible with the CHARMM all-atom additive biological force fields. *J. Comput. Chem.* **2010**, *31* (4), 671−690.

(33) Ross, G. A.; Rustenburg, A. S.; Grinaway, P. B.; Fass, J.; Chodera, J. D. Biomolecular simulations under realistic macroscopic salt conditions. *J. Phys. Chem. B* **2018**, *122* (21), 5466−5486.

(34) Helal, M. A.; Shouman, S.; Abdelwaly, A.; Elmehrath, A. O.; Essawy, M.; Sayed, S. M.; Saleh, A. H.; El-Badri, N. Molecular basis of the potential interaction of SARS-CoV-2 spike protein to CD147 in COVID-19 associated-lymphopenia. *J. Biomol. Struct. Dyn.* **2022**, *40* (3), 1109−1119.

(35) Golo, V.; ShaItan, K. Dynamic attractor for the Berendsen thermostat an the slow dynamics of biomacromolecules. *Biofizika* **2002**, *47* (4), 611−617.

(36) Tuble, S. C.; Anwar, J.; Gale, J. D. An approach to developing a force field for molecular simulation of martensitic phase transitions between phases with subtle differences in energy and structure. *J. Am. Chem. Soc.* **2004**, *126* (1), 396−405.

(37) Darden, T.; York, D.; Pedersen, L. Particle mesh Ewald: An N·log (N) method for Ewald sums in large systems. *J. Chem. Phys.* **1993**, *98* (12), 10089−10092.

(38) Mori, K.; Matsumoto, N.; Nomoto, S.; Tsuruta, K. Computational and experimental analyses of detachment force at the interface between carbon fibers and epoxy resin. *Open J. Compos. Mater.* **2017**, *7* (4), 179−184.

(39) Pall, S.; Hess, B. A flexible algorithm for calculating pair interactions on SIMD architectures. *Comput. Phys. Commun.* **2013**, *184* (12), 2641−2650.

https://doi.org/10.1021/acsomega.3c09355
ACS Omega 2024, 9, 14005−14016